Efficient Time-Domain Focussing for General Bistatic SAR Configurations: Bistatic Fast Factorised Backprojection

Marc Rodriguez-Cassola, Pau Prats, Gerhard Krieger, Alberto Moreira
Microwaves and Radar Institute, German Aerospace Center (DLR), 82234 Wessling, Germany

Abstract

Due to the lack of an appropriate symmetry in the acquisition geometry, generalised bistatic SAR cannot benefit from the two main properties of low-to-moderate resolution monostatic SAR: azimuth-invariance and topography-insensitivity. Precise accommodation of azimuth-variance and topography is a real challenge for efficent algorithms working in the Fourier-domain, but can be quite naturally handled by time-domain approaches. We report about the first efficient and practical implementation of a generalised bistatic SAR imaging algorithm with an accurate accommodation of these two effects. The algorithm has a common structure with the monostatic fast factorised backprojection (FFBP), and is therefore based on subaperture processing. The algorithm is tested with both simulated and actual bistatic SAR data. The actual data correspond to the spaceborne-airborne experiment between TerraSAR-X and F-SAR performed in 2007. The presented approach proves its suitability for precise imaging of any given scene acquired by any given bistatic SAR configuration.

1 Introduction

Bistatic SAR imaging complexity has often been only approximately addressed in the recent literature. In an analogous manner to the development of monostatic SAR imaging algorithms, improvements in precision and computational efficiency have become available over time. Normal as this evolution might seem, the accessible knowledge has sometimes been ignored in new developments. Most popular fast monostatic SAR imaging algorithms rely on the assumptions of linear trajectories, constant height and constant spatial sampling (velocity of the platform divided by pulse repetition frequency) of the system. For a ranging system such as a radar, the previous assumptions impose in the acquisition geometry a circular cylindrical symmetry essential for understanding the existing imaging approaches: targets placed on a given circular cylinder share the same reference range history to the radar, shifted proportionally to the along-track position of the target. Two essential properties emanate from this advantageous symmetry: a) azimuth-invariance, and b) insensitivity to topography. The former guarantees that focussing can be performed efficiently in the Fourier-domain, since imaging is achieved by range history correlation. The latter allows a precise computation of range histories with the sole knowledge of target delays, independently on the three-dimensional (3D) position of the target with respect to the radar. The conclusion is that precise efficient focussing can be accomplished independently of the imaged scene. Among bistatic SAR configurations, a straightforward classification depending on their geometric symmetry (and proximity to the ideal monostatic case) can be established.

- The constant equal velocities, same track and along-track offset case shows exactly the same circular cylindrical symmetry as the monostatic case. This configuration shares the azimuth-invariance and the topography-insensitivity of ideal monostatic SAR.

- The constant equal velocities and parallel tracks case has elliptical cylindrical symmetry. The configuration is azimuth-invariant (for a flat constant range line) and topography-sensitive.

- Any other bistatic configuration is, in general, azimuth-variant and topography-sensitive.

In other words, even if the approximation of linear trajectories is assumed, bistatic SAR imaging algorithms need take into account the topographic changes of the imaged scene. The spatial-variance introduced by realistic topography scenarios in the SAR system response might be difficult to accommodate in efficient implementations of Fourier-domain algorithms. One natural solution to accommodate the azimuth-variance and topography-sensitivity of bistatic SAR is focussing in the time-domain using the backprojection algorithm (BP). However, the real drawback that makes the use of BP non-feasible is the large computational burden it requires. This paper proposes an imaging algorithm for bistatic SAR based on the fast factorised backprojection algorithm [1], and is therefore named bistatic fast factorised backprojection (BFFBP). Partial results of the algorithm were already addressed in [2]. A deeper analysis of the algorithm is presented in [3]. In the following pages, fundamental issues of BFFBP like the image coordinate system, the Nyquist requirements or even implementations hints are discussed. Moreover, the algorithm is tested with simulated and real bistatic data.

2 Geometric model

The geometric model of the analysed bistatic configuration only assumes a transmitter and a receiver. No linear, nor parallel, nor constant-speed trajectories are needed to achieve precise focussing. Due to the difficulty of drawing a general intuitive picture, we will use Fig. 1 as illustration of the geometric model. Despite its lack of generality, we have chosen the geometry of a spaceborne-airborne bistatic SAR configuration because it encompasses many of the issues only backprojection algorithms can deal with in a precise manner. Note that the algorithm is able to handle bistatic data of any other configuration (spaceborne-spaceborne, airborne-airborne, one-stationary) up to any desired resolution within the physical constraints of electromagnetic imaging.

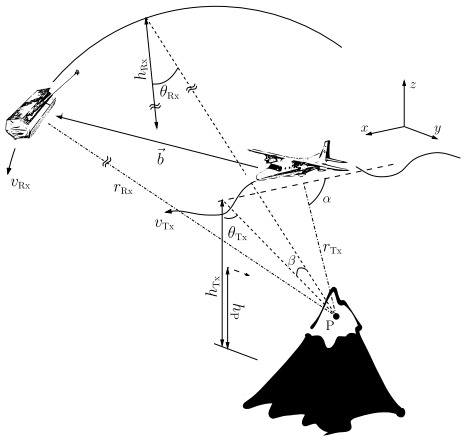

Figure 1: Bistatic spaceborne-airborne configuration used as an illustrative case of a general bistatic SAR configuration.

3 Bistatic fast factorised backprojection (BFFBP)

As already stated, this bistatic version of the algorithm fast factorised backprojection [1] achieves precise accommodation of azimuth-variance and topography of general bistatic SAR acquisitions, while keeping a speed-up factor proportional to $\log_2 N$ with respect to direct backprojection (DBP), in a similar manner as Fourier-domain algorithms do.

3.1 Image reference system

The reference system for subimage computations has an elliptical range coordinate and an angular coordinate referenced to the transmitter trajectory (but might as well be defined to the receiver's, if convenient). This reference system, shown in Fig. 2 in the general case, keeps the advantage of lowest bandwidth images while offering an advantageous manner of displaying topography information.

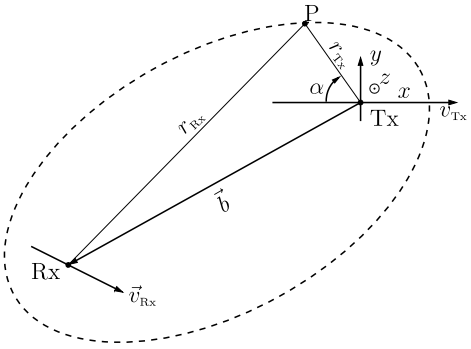

Figure 2: Reference grid used in BFFBP.

3.2 Nyquist requirements

Due to the space-variant character of bistatic SAR, the angular Nyquist requirements vary for different subapertures and even within a bistatic image. This effect might force to the need of a numerical evaluation of the Nyquist requirements every time a subaperture is processed, which might result in additional significant computational burden. A safe bound for the angular sampling requirement for general SAR configurations is

$$\delta(\cos\alpha) \geq \left| \frac{\lambda - |\omega_{\mathrm{Rx},y} \cdot k|}{T \cdot r_{\mathrm{Tx}} \cdot (\omega_{\mathrm{Tx}} + \omega_{\mathrm{Rx},x})} \right| , \qquad (1)$$

where λ is the radar wavelength, T is the duration of the synthetic aperture, r_{Tx} is the range transmitter-target, ω_{Tx} is transmitter's instantaneous angular velocity, and $\omega_{\mathrm{Rx},x}$ and $\omega_{\mathrm{Rx},y}$ are the x and y components, respectively, of receiver's intantaneous angular velocity, and k is a constant which depends on the geometry of the acquisition. A more detailed analysis on the obtention of (1) can be found in [3]. We remind that the instantaneous angular velocity reaches its maximum v/r_0 at monostatic zero-Doppler time and decreases to zero for high-squinted monostatic positions. The numerical estimation of the worst cases for the instantaneous angular velocities is easy to implement, but (1) can be again bounded by including the maximum values of transmitter's and the x component of receiver's angular velocities if necessary. By setting $\omega_{\mathrm{Rx},y} = 0$, we obtain the compact expression of the angular Nyquist requirement of bistatic general along-track acquisitions

$$\delta(\cos\alpha) \geq \frac{\lambda}{T \cdot r_{\mathrm{Tx}} \cdot (\omega_{\mathrm{Tx}} + \omega_{\mathrm{Rx}})} . \qquad (2)$$

The influence of the $\omega_{\mathrm{Rx},y}$ is somewhat more complex to quantify, since values close to the wavelength reduce the information content of (1). Whenever this happens, we need to evaluate the expressions leading to (1) to derive an estimate of the angular sampling condition [3].

3.3 Implementation and computational burden

BFFBP is implemented analogously to FFBP [1], however accounting for the different reference system and Nyquist requirements. The first stage of the algorithm is the computation of the scene topography in a convenient coordinate system. A very advantageous solution is a regular monostatic backgeocoding of the imaged scene. Note that the elliptical grids only contain monostatic angular information. After this, the algorithm enters its recursive kernel, where the aperture is factorised or regular DBP for the considered subaperture is computed. Every factorisation of the input data requires a split of the radar trajectories and a computation of new lower-resolution elliptical grids. The computation of DBP on the lowest-resolution elliptical grid outputs back to the previous stage of recursion, where all the subimages are interpolated into the higher-resolution elliptical grids. This interpolation is the main error source of BFFBP, provided that all Nyquist requirements are fulfilled, and must be carried out carefully. Unfortunately, it is also the computational bottleneck of the algorithm. After interpolation of two consecutive higher-resolution subimages, the algorithm goes back another stage and repeats. Note that the interpolation of increasing resolution polar grids is one of the highlights of [1], since it minimises the number of required interpolations by always computing subimages on the best possible working grids. We keep this essential feature in our implementation by always using elliptical grids for the subimage computations. Moreover, since all elliptical grids contain the topographic information of the scene up to the required resolution, topography accommodation is naturally achieved in the increasing resolution subimages. Another advantage of FFBP over other Fourier-domain algorithms is the small number of points of the subapertures.

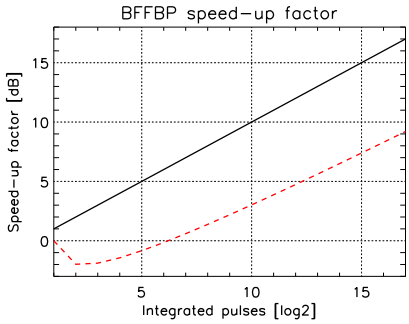

Figure 3: BFFBP speed-up factor: $\log_2$ speed-up factor (solid), eight-point truncated sinc (dashed).

FFBP can start backprojecting low-resolution subimages during the acquisition, the time any other Fourier-domain algorithm remains idle. Using analogous logic, the memory requirements of the FFBP approach a factor 2 benefit with respect to Fourier-domain techniques, since the data used to backproject low-resolution subimages can readily be discarded before grid interpolation. Last but not least, the effect of working on a pulse-to-pulse basis makes FFBP a good candidate for multithreaded implementations benefitting from the multicore technology used in almost any CPU produced nowadays. Fig. 3 shows the $\log_2$ of the speed-up factor for a 2D eight-point truncated sinc interpolation kernel (dashed). This speed-up factor is proportional to $\log_2 N_a$, the behaviour of monostatic FFBP using lower-order interpolators, which is also depicted in Fig. 3 (solid).

3.4 Experimental results

3.4.1 Simulated data

A total of four point targets distributed all over Barcelona metropolitan area are generated using the translated motion data of the DLR TerraSAR-X/F-SAR spaceborne-airborne experiment [4] at a modified height, 1167 m. Setting the targets in Barcelona has the advantage of having a modest topographic profile which allows to test the ability of the algorithm to accommodate the topographic changes of a realistic scenario. The selected point targets, positions and heights are listed in Table 1.

Table 1: Point targets position of Barcelona simulation

Ref.	Latitude	Longitude	Height
P1	45.81239°	43.0027°	12.9 m
P2	45.8161°	42.6756°	37.5 m
P3	45.80449°	42.9029°	36.7 m
P4	45.85781°	42.6898°	409.8 m

Table 2: Parameters used in simulated data synthesis

Integration time [s]	3.2768
Pulse repetition frequency [kHz]	10
Ground range scene length [m]	6575
Azimuth scene length [m]	4400
Wavelength [m]	0.031
Transmitted bandwidth [MHz]	300
TerraSAR-X velocity [m/s]	7408
F-SAR velocity [m/s]	90
TerraSAR-X altitude [km]	514
F-SAR altitude [m]	1167

The expected along-track resolutions for all point targets are modest (46.4, 53.4, 48.9, and 52.9 cm for P1 to P4, respectively; significantly better along-track resolutions were obtained in [4]), but they are sufficient for the exemplary purpose. The version of BFFBP without topographic accommodation consists of a full BFFBP processing using a constant height model of 225 m. BFFBP over this flat grid can be thought of as a higher bound for any Fourier-domain bistatic SAR processing algorithm willing to flee from costly space-variant wide-bandwidth corrections, since precise focussing for the assumed DEM is

achieved. The focussed responses with and without topography accommodation are shown in figures 4 and 5, respectively. Significant defocussing, even for the ordinary values of the simulation, is found in targets 1 and 3 (located at nearer range) in the case of BFFBP over the flat grid.

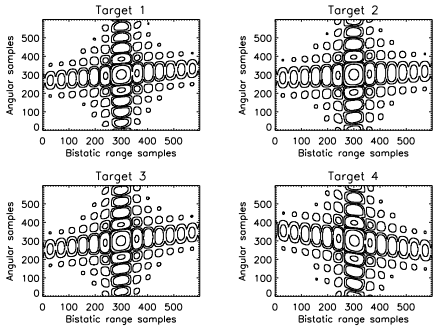

Figure 4: Simulated point target responses using BFFBP with topography accommodation (realistic external DEM).

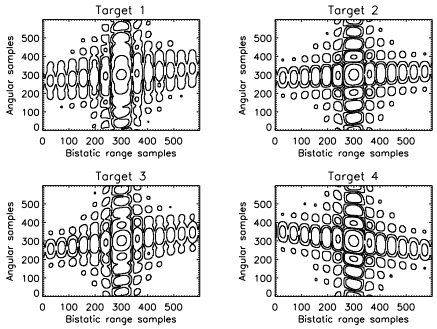

Figure 5: Simulated point target responses using BFFBP without topography accommodation (flat DEM at 225 m height).

3.4.2 First experiment TerraSAR-X/F-SAR

A complete overview on the first experiment TerraSAR-X/F-SAR, performed early November 2007, can be found in [4]. The bistatic image obtained using BFFBP is shown in Fig. 6.

4 Summary

The paper has presented the first efficient approach to bistatic SAR imaging capable of precisely accommodating azimuth-variance and topography-dependence, the two main challenging issues in general bistatic configurations. The algorithm, based on a subaperture approach, is also well suited for parallelised and real-time implementations, independent of radar wavelength, scene size or desired resolution. It follows the framework of the monostatic fast factorised backprojection algorithm, but extends its suitability for general bistatic configurations by presenting an advantageous image coordinate system. A bistatic image processed with BFFBP has also been presented.

Figure 6: BFFBP-processed bistatic image of the TerraSAR-X/F-SAR first spaceborne-airborne experiment. Radar illumination from the bottom.

References

[1] L. Ulander *et* al, 'Synthetic-aperture radar processing using fast factorized back-projection', *IEEE Trans. Aerosp. Electr Syst.*, vol. 39, no. 3, pp. 760-776, Jul. 2003.

[2] M. Rodriguez-Cassola *et* al, *New processing approach and results for bistatic TerraSAR-X/F-SAR spaceborne-airborne experiments*, Proc. IGARSS 2009, Cape Town, South Africa.

[3] M. Rodriguez-Cassola *et* al, 'Efficient Time-Domain Image Formation with Precise Topography Accommodation for General Bistatic SAR Configurations', submitted to *IEEE Trans. Aeros. Electr. Syst.*

[4] M. Rodriguez-Cassola *et* al, 'Bistatic TerraSAR-X/F-SAR spaceborne-airborne SAR experiment: description, data processing and results', *IEEE Trans. Geosci. Remote Sens.*, vol. 48, no. 2, pp. 781-794, Feb. 2010.